electricity

MDPI

Article

Stability Enhancement of a Multi-Source Interconnected Power System Using a Dung Beetle Optimizer-Tuned $PI^{\lambda}D^{\mu}$ Controller

Boopathi Dhanasekaran [1,*], Jagatheesan Kaliannan [2], Sathish Kumar Marappan [3], Sourav Samanta [4] and Anand Baskaran [5]

1 Department of Electrical and Electronics Engineering, Paavai Engineering College, Namakkal 637018, Tamil Nadu, India
2 Department of Electrical and Electronics Engineering, Vivekanandha College of Engineering for Women, Namakkal 637205, Tamil Nadu, India; jaga.ksr@gmail.com
3 Department of Mathematics, Paavai Engineering College, Namakkal 637018, Tamil Nadu, India; msksjv@gmail.com
4 Department of Computer Science Engineering, University Institute of Technology, The University of Burdwan, Burdwan 713104, Westbengal, India; sourav.uit@gmail.com
5 Department of Electronics and Instrumentation Engineering, Hindusthan College of Engineering and Technology, Coimbatore 641032, Tamil Nadu, India; anand.eie@hicet.ac.in
* Correspondence: boopathime@gmail.com

Abstract

Maintaining frequency stability in modern interconnected power systems (PSs) has become increasingly challenging due to the high penetration of renewable energy sources (RESs) and the dynamic nature of generation and demand. To address these issues, this paper proposes a novel load frequency control strategy that integrates a Dung Beetle Optimizer (DBO)-tuned fractional-order Proportional–Integral–Derivative (FOPID) controller with a newly developed multi-source interconnected power system. This model combines PV, thermal, hydro, nuclear, and advanced storage (HAE and fuel cells). Unlike existing methods, the proposed approach simultaneously leverages DBO's balanced search mechanism and FOPID's fractional dynamics to enhance frequency stability under high renewable penetration. The performance of the proposed controller is validated through a comparative analysis with Ant Lion Optimizer (ALO) and Particle Swarm Optimization (PSO) methods. Simulation results show that the DBO-based controller significantly improves dynamic response, achieving reductions in settling time of 9.5% and 4.7% compared to PSO and ALO, respectively. Furthermore, the proposed approach enhances frequency regulation and tie-line power stability over other optimization methods and controllers, demonstrating strong robustness and adaptability for future high-RES power systems.

Keywords: factional order controller; frequency stability; dung beetle optimizer; ant lion optimizer; particle swarm optimization

Check for updates

Academic Editor: Andreas Sumper

Received: 7 June 2026
Revised: 24 July 2026
Accepted: 29 July 2026
Published: 5 August 2026

Copyright: © 2026 by the authors. Licensee MDPI, Basel, Switzerland. This article is an open access article distributed under the terms and conditions of the Creative Commons Attribution (CC BY) license.

1. Introduction

The rising need for electricity has prompted the development of a variety of generation methods, while traditional sources such as thermal, hydro, nuclear, and diesel remain prevalent, they are environmentally harmful due to pollutant emissions. To address this, renewable energy sources (RESs) such as solar, wind, biogas, and geothermal are increasingly being used, frequently with smaller-scale power units. Power centralization, achieved by integrating power systems (PSs) into a common grid, enables efficient load

balancing and a reliable power supply. However, rapid variations in load demand on the grid can cause frequency fluctuations.

Load frequency control (LFC) is used to manage these variances while maintaining stability. Proportional (P), Integral (I), and Derivative (D) (PID) controllers are frequently utilized in LFC because they are simple and effective. However, there is a rising awareness of the importance of optimizing PID settings to address system uncertainties and increase performance in dynamic conditions. Various optimization algorithms have obtained optimal PID controller parameters to enhance system stability. The classical PID, PI, PD controllers were used by many of the researchers, but the efficacy of the classical controller has not been sufficient for impulses in the power line. In [1], a self-adaptive PID controller was proposed and optimized by particle swarm optimization (PSO), and the simulation result was compared with the Hopfield neural network-based PID controller. The dynamic response of a dual PS with a PSO–PID controller was investigated in [2] and the simulation response compared with GA. In [3], a PS-PID controller optimized by Ant Colony Optimization was used in a standalone wind turbine to linearize the power output, and the superiority of the proposed optimization method was demonstrated by comparing the results with those of the PSO method. The authors incorporated the Grasshopper Optimization Algorithm and PSO of [4] to optimize the PID controller in a single- and dual-area PS. A cascade PI–PD controller designed and optimized by Harris Hawks' optimizer to stabilize the frequency difference due to the load change in the power grid was investigated by [5]. Using the same PSO technique as for a single-area PS, the authors of [6] performed analyses under various loading conditions and with various PS capacities.

Conventional PID controllers have been widely used for LFC, but recent studies have shifted toward fractional-order variants for greater tuning flexibility and robustness. For instance, in [7], the Global Neighborhood Algorithm was utilized to develop an FOPI-FOPID controller for AGC in single/multi-area PSs. Several recent studies have investigated using FOPID controllers for LFC in various PS configurations like hydro, solar, thermal, and zero-carbon PSs [8], Electrical Vehicle (EV)-integrated thermal PS [9], non-reheated thermal PS [10], Microgrid, which includes solar, wind, and diesel PSs [11], and a four-area PS constructed with thermal, hydro, and PV [12].

In [13], the author introduced a novel optimization technique called Jellyfish Search to tune three different controllers for an interconnected PSs with three areas of unequal power sources in LFC. Another optimization technique, Atom Search Optimization, was applied to tune the FOPID controller for a hybrid PSs [14], and its stability performance was analyzed. PS stability was achieved using a fuzzy FOPID controller tuned by the biogeography-based optimization technique [15]. The Big Bang Big Crunch approach was used for the stability process of a multiple-area PS, incorporating the effect of the Super Magnetic Energy Storage unit [16]. For LFC in a thermal-hydro PS with non-linear constraints, as in [17], a FOPID controller was tuned using the Teaching-Learning-Based Optimization (TLBO) technique. Furthermore, the performance of the controller was compared with TLBO-PID, demonstrating that the proposed controller offers an improved response. A study was conducted on a PS fully designed on renewable energy sources [18]. Furthermore, in a multiple-source integrated PS, frequency oscillation is controlled by using a PSO-optimized FOPID controller [19]. A nonlinear FOPID controller was employed. The controller gain parameters of a FOPID controller were optimized using the Cohort Intelligence Optimization in [20] to achieve improved response in thermal PS. A single area including multiple sources is investigated by PSO–PID controller [21]. for the same PSs with four different objective functions, namely IAE, ISE, ITAE, and ITSE [22].

The Sine Cosine Algorithm was developed for an interconnected PS comprising thermal, hydro, gas, wind, and pumped-energy storage (ESS) systems [23]. The author

of [24] proposed a cascade fuzzy FOPID controller. Furthermore, a Seagull Optimization Algorithm- [25], Grey Wolf Optimizer- [26], Imperialist Competitive Algorithm [27] optimized FOPID controller was suggested for an interconnected thermal PS to control frequency oscillation; the performance was compared with other famous robust controllers. A multiple-source interconnected PS was investigated in [28] using an FOPID-FOPI controller for LFC, with reliability and durability assessed through robustness tests involving parameter and load changes. In a hybrid PS consisting of thermal, wind, and solar sources, a Moth Flame Optimization-based Generalized Hopfield Neural Network-based FOPID controller was employed for LFC [29]. For the same system, a modified derivative controller was designed by [30] to fight against frequency oscillation. A protection for the Egyptian PS in 2035, which is dominated by RESs, is investigated with a Runge–Kutta optimizer-based FOPID controller, and its response was noticeable against frequency fluctuation [31].

In [32], a fractional controller was designed for LFC in an interconnected PS, and its response was compared with that of a PID controller as well as the open-loop response. The LFC was performed using a multi-objective optimization-based FOPID controller, and its robustness was assessed through the application of random load variations [33]. The African Vulture Optimization Algorithm was utilized to tune a FOPID controller designed for LFC, and its performance was compared with that of FOTID and FOD controllers [34]. The frequency control problem of a hybrid PS is smoothly handled by introducing a novel controller called the Interline Power Flow Controller [35]; the dynamic performance is well controlled over other famous controllers. Incorporating renewable energy sources raises many challenges like nonlinear outputs, but significantly, this reduces CO_2 emissions [36].

1.1. Motivation and the Research Gap

A comprehensive survey conducted on the implementation of LFC in PSs has provided valuable insights into the influence of secondary controllers and the methods used for tuning these controllers. Various optimization techniques and algorithms, such as GA, PSO, GOA, TLBO, GWO, MFO, AVOA, and other popular algorithms, have been applied by researchers to overcome the frequency oscillation problems with significant advancements. However, a specific research gap was identified, which prompted the development of a sophisticated PS and the implementation of an FOPID controller tuned by the DBO technique to address this gap.

1.2. Challenges of This Work

Even though the FOPID controller has provided sufficient outcomes for the frequency deviation problem, it encounters a few challenges when implemented in a complex power network.

1. Facing nonlinearity is a major challenge because of renewable energy sources and unexpected load changes.
2. Optimizing 5D parameters for the FOPID controller, such as K_P, K_I, K_D, λ, and μ, is too difficult.

1.3. The Key Contributions of This Study

1. Development of a comprehensive multi-source interconnected PS comprising thermal, nuclear, hydro, and PV power sources integrated with advanced ESS technologies (HAE, FC).
2. Design and implementation of a DBO-tuned FOPID controller, tailored for the dynamic characteristics of the proposed multi-source PS, to obtain robust and precise frequency stability under diverse operating conditions.

3. Comprehensive comparative analysis of PD, PID, and FOPID controllers optimized using three different metaheuristic algorithms—PSO, ALO, and DBO—to evaluate their impact on frequency stability and dynamic performance.
4. Demonstration of the superior performance of the DBO–FOPID controller, achieving the lowest settling time and overshoot among all tested configurations, thereby confirming its robustness and effectiveness for interconnected multi-source PS.

1.4. Structure of the Article

The proposed study is structured as follows: Section 1 introduces the concept of LFC, along with the necessity of implementing a secondary controller for the PSs being studied. Section 2 provides a detailed explanation of the developed PSs. The design of the controller and its features are discussed in Section 3. Section 4 focuses on the Dung Beetle Optimizer and the optimized controller parameters. To validate the effectiveness of the DBO optimizer in comparison to other methods, Section 5 presents a thorough discussion of the results. Finally, Section 6 presents the study's conclusion.

2. System Model to Investigate

This study examines the analysis of an advanced power system (PS) design. The system consists of major large-scale power generation units such as thermal, nuclear, and hydropower plants, along with the integration of PV and energy storage systems (ESS), including hydrogen aqua energy (HAE) and fuel cells (FC). The growing use of renewable energy sources (RESs) in recent years is intended to reduce carbon emissions and tackle the shortage of fossil fuels. The overall model is shown in Figure 1.

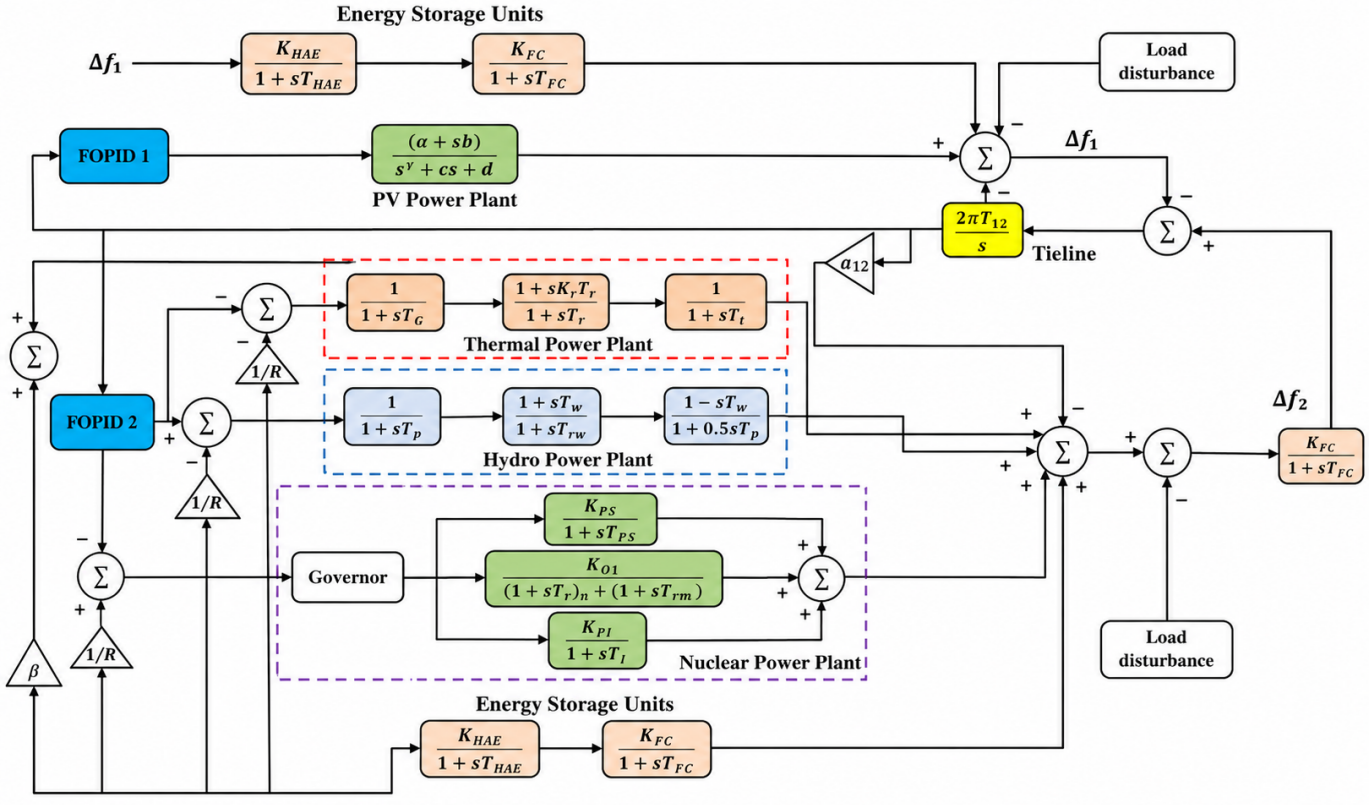


Figure 1. Proposed sophisticated PS model.

2.1. Thermal Power Plant

Thermal power generation is among the leading methods used for large-scale electricity production across the globe, especially in developing nations. A thermal power plant generally comprises several essential components: a governor that regulates steam flow into the turbine, a steam turbine that transforms steam pressure into mechanical energy, and a reheater that reheats the outlet steam from the turbine [37]. A diagram illustrating the block diagram of a conventional thermal PS is presented in Figure 2. Therein, T_G, T_r, and T_T are the time constants of the governor, reheater, and turbine. K_r is the time constant of the reheater; this constant was used to develop a mathematical model of the thermal power plant. Whereas U(t) is the control signal from the secondary controller to the plant to regulate the input to the plant.

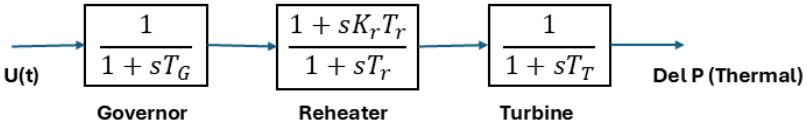


Figure 2. Conventional thermal power plant block diagram.

2.2. Hydropower Plant

Hydropower, also known as hydroelectricity, is a method of generating electricity by harnessing the energy of flowing or rapidly moving water through turbines that drive generators. The hydro plant has a mechanical governor and a hydro turbine. The governor is used to regulate the input of the turbine, which changes the speed of the turbine. We correlate with the speed and frequency. As of 2019, hydroelectric power contributed more than 18% of the global power-generating capacity [21]. The block diagram of a hydropower facility is illustrated in Figure 3. Therein, T_H, T_{GH}, and T_W are the time constants of the governor and hydro turbine.

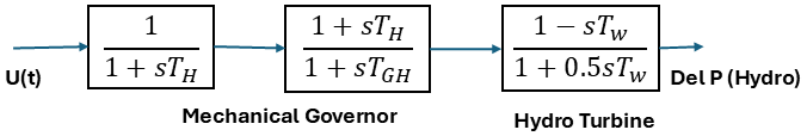


Figure 3. Conventional hydropower plant block diagram.

2.3. Nuclear Power Plant

In developing nations, the growing demand for electrical power drives the adoption of nuclear power plants as an alternative to conventional generation methods. Nuclear power provides the benefit of generating substantial amounts of electricity from a comparatively small quantity of nuclear fuel. A nuclear PS is made up of two main components: a speed governor and a turbine. In this study, a mathematical model of a tandem compound turbine is employed. The tandem compound turbine consists of a high-pressure (HP) turbine and two low-pressure (LP) turbines. The primary role of the HP turbine is to lower steam moisture before it reaches the LP turbines, thereby reducing erosion rates within the turbine [38] The modeling of the nuclear PS was developed for investigative purposes. Figure 4 illustrates an isolated nuclear PS setup [21]. In Figure 4, T_{T1}, T_{RH1}, T_{RH2} are the time constants of low- and high-pressure turbines and K_{H1} & K_{R1} are turbine gain constants, respectively.

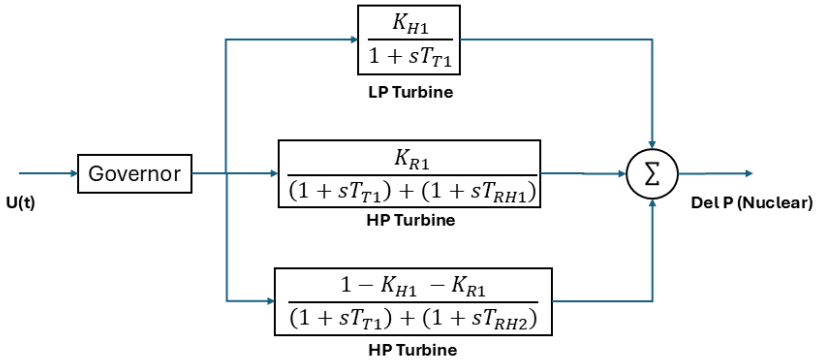


Figure 4. Conventional nuclear plant block diagram.

2.4. Solar PV Power Plant

In the analyzed system, the solar PV grid serves as area 2 and is linked to area 1. As shown in Figure 5, the PV cell model consists of a current source in parallel with a diode (D) and a modest resistance (R) in series with the solar cell terminals. The current source is determined by the amount of sunshine (radiation) and the temperature.

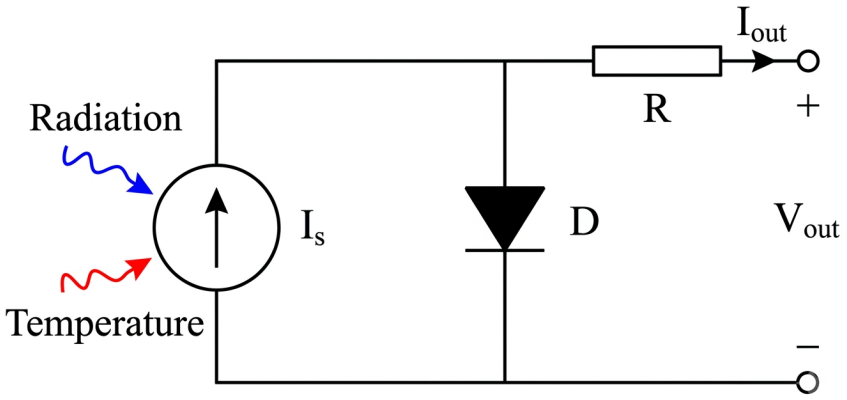


Figure 5. Solar PV cell equivalent circuit.

Depending on the temperature and amount of radiation that the solar panels receive, their output voltage and power generation fluctuate throughout the day. In solar PV systems, maximum power point tracking (MPPT) is a useful implementation that helps identify the panel's operating point at peak power. By adjusting the power converter's duty cycle to a specific value, the power extracted from the panel can be optimized even in the face of significant variations in meteorological circumstances. Therefore, this work uses MPPT in the modeling to optimize power extraction from the solar PV system. The transfer function of solar PV is given in Equation (1).

$$G_{pv}(s) = \frac{-18s + 900}{s^2 + 100s + 50} \tag{1}$$

2.5. ESS Units

In the investigated PS, energy storage units (HAE and FC) are employed to assist in balancing minor power demands without requiring significant changes in generation parameters. These energy storage units offer valuable support to the secondary controller within the proposed power network. A system comprising an HAE, a hydrogen storage tank, and an FC is utilized to fulfill long-term and large-scale load demands. The HAE produces hydrogen (H_2) through water electrolysis using electricity, which is then compressed and stored in the tank for future use. Proton exchange membrane fuel cells

(FCs) utilize the stored hydrogen to generate on-site energy, thereby meeting peak loads. This process results in high efficiency due to the utilization of multiple energy conversion methods. Additionally, water and heat are by-products of this process [30]. Under normal operating conditions, the proposed energy storage unit operates as a load by absorbing excess energy. During sudden increases in load demand, the energy storage unit acts as a source, supplying the required amount of energy to support the system. This enables the system to maintain stability and ensures good power quality during transient operating conditions. The parameters in the transfer function of the ESS, K_{HAE} and K_{FC} are the time constants of HAE and FC, respectively. Similarly, T_{HAE} and T_{FC} are the time constants of HAE and FC, respectively.

3. Fractional PID Controller Design

Podlubny proposed the FOPID controller, which has attracted considerable interest owing to its superior performance relative to classical PID controllers. This controller provides greater design flexibility through five tunable parameters, enabling improved shaping of the open-loop transfer function to meet specific control needs. A wide range of studies in the literature have shown the benefits of FOPID controllers over PID controllers for both integer and fractional order systems. However, tuning and designing FOPID controllers is more intricate, necessitating stability analysis and dedicated design approaches. Equation (2) shows the transfer function of the FOPID controller, where specific values of λ and μ yield different standard controller types: $\lambda = 1$, $\mu = 1$ for a standard PID controller, $\lambda = 1$, $\mu = 0$ for a standard PI controller, $\lambda = 0$, $\mu = 1$ for a standard PD controller, and $\lambda = 0$, $\mu = 0$ for a standard P controller.

$$G_c(s) = K_P + \frac{K_I}{s^\lambda} + K_D s^\mu \tag{2}$$

When tuning controller gain parameters through optimization techniques, the tuner sets parameter boundaries according to the specific application. The goal is to minimize the performance index (J) and adjust the controller gain parameters accordingly. Figure 6 shows the typical structure of an FOPID controller [39].

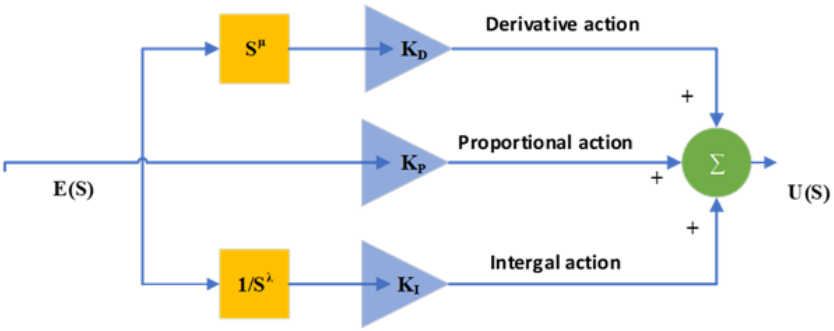


Figure 6. Typical structure of FOPID controller.

Key Features of FOPID

Improved Performance: When compared to traditional PID controllers, FOPID controllers can frequently achieve superior dynamic performance, which results in the following:

- **Decreased overshoot/undershoot:** Following a disturbance, there is less variation in frequency and tie-line power.
- **Faster settling time:** It takes less time for the system to stabilize. Better resilience to abrupt demand variations or intermittent renewable energy sources (such as variations in wind or solar power) is known as improved disturbance rejection.

- **Enhanced Robustness:** FOPID controllers are typically more resilient to ambiguities and changes in PS characteristics, such as shifts in generator inertia and turbine time constants. Given the growing integration of distributed generation and renewable energy sources, which can increase fluctuation, this is especially crucial in contemporary power systems.
- **Improved Management of Complex Dynamics:** The PS dynamics are complex, frequently non-linear, and fractional-order-like. By their very nature, FOPID controllers are more capable than integer-order controllers of capturing and reacting to these complex phenomena.

4. Dung Beetle Optimizer

4.1. Fundamentals of DBO

The DBO algorithm is a novel population-based intelligence technique inspired by the behavior of dung beetles, which involves activities such as rolling a ball, foraging, dancing, reproducing, and snatching. In the proposed algorithm, each cluster of dung beetles comprises four distinct agents, including a small dung beetle and a burglar that rolls its offspring in a ball-like manner. Equation (3) is utilized to calculate the coordinates of the manure beetle, and Equation (4) is used to simulate fluctuations of light intensity.

$$x_i(t+1) = x_i(t) + \alpha k\, x_i(t-1) + b\, \Delta x \tag{3}$$

$$\Delta x = \left| x_i(t) - X^w \right| \tag{4}$$

where

- t—number of iterations;
- x_i(t)—ith dung beetle position at the t^{th} iteration;
- k ∈ [0, 0.2]—constant values of deflection coefficient;
- b—constant value (0, 1);
- α—natural coefficient (which is assigned -1 or 1);
- X^w—global worst position;
- Δ_x—simulate fluctuations of light intensity.

The revised and redefined position for the ball-rolling dung beetle is represented by Equation (5) as follows. Where θ is the deflection angle fitting to [0, π] and X^* is the present local best position.

$$x_i(t+1) = x_i(t) + \tan(\theta) \left| x_i(t) - x_i(t-1) \right| \tag{5}$$

A boundary range method is devised to emulate the egg-laying locations of female dung beetles, which is defined by Equations (6) and (7). Lb^* and Ub^* are lower and upper boundaries of the depositing area, respectively. R = 1 − t/T_{max}, where T_{max} is the maximum iteration number. Lb and Ub are the lower and upper boundaries in optimization problems.

$$Lb^* = \mathrm{mix}(X^* \times (1-R) \cdot Lb) \tag{6}$$

$$Ub^* = \min(X^* \times (1+R) \cdot Ub) \tag{7}$$

In the iteration process, the position of the brood ball also plays a crucial role, and it is represented by Equation (8). In Equation (8), $B_i(t)$ denotes i^{th} brood ball position at t^{th} iteration, b_1 and b_2 are independent random vectors, and D is the size of optimization

issues. In Equations (9) and (10), X^b denotes global, Lb_b and Ub_b are optimal foraging areas (lower and upper).

$$B_i(t+1) = X^* + b_1 \times \left(B_i(t) - Lb^*\right) + b_2 \times \left(B_i(t) - Ub^*\right) \quad (8)$$

The boundary of the optimal foraging area is defined and presented in Equations (9) and (10) as follows:

$$Lb^b = \text{mix}(X^* \times (1-R) \cdot Lb) \quad (9)$$

$$Ub^b = \min(X^* \times (1+R) \cdot Ub) \quad (10)$$

The position of the small dung beetle is continuously updated, and this process is described by Equation (11). Where x_i (t) is i^{th} little beetle position at the t^{th} iteration, C_1 and C_2 are random number (0, 1). Equation (12) express the thief's position information updated. Where x_i (t) is the i^{th} thief position at the t^{th} iteration, g is a Random vector of size 1 × D, and S is denoted as a constant.

$$x_i(t+1) = x_i(t) + C_1\left(x_i(t) - Lb^b\right) + C_2\left(x_i(t) - Ub^b\right) \quad (11)$$

$$x_i(t+1) = X^b + S \times g \times \left(|x_i(t) - X^*| + |x_i(t) - X^b| \right) \quad (12)$$

Throughout the optimization process, the positions of the ball-rolling dung beetle, brood ball, little dung beetle, and thief are continuously modified. At the end of the process, the best position is identified, and the corresponding values of Xb and fitness are output. Flow chart of DBO is shown in Figure 7 and fitness convergence of optimization techniques is given in Figure 8.

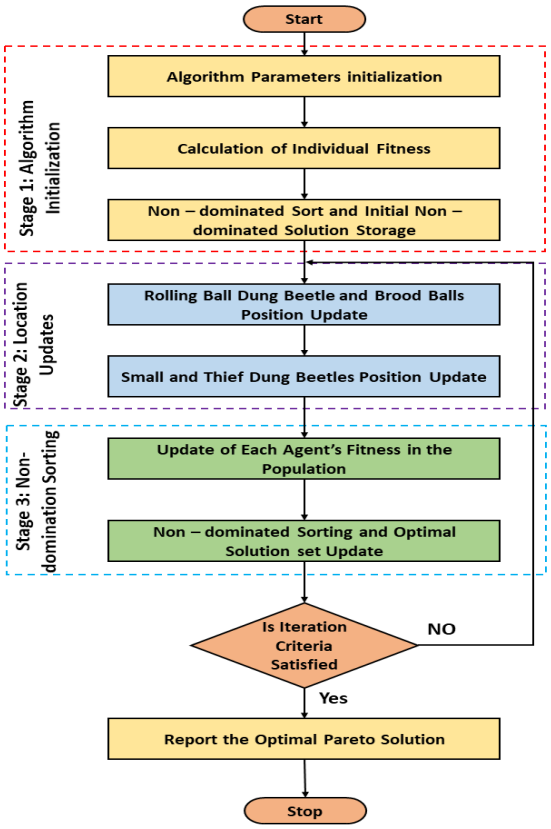


Figure 7. DBO flow chart.

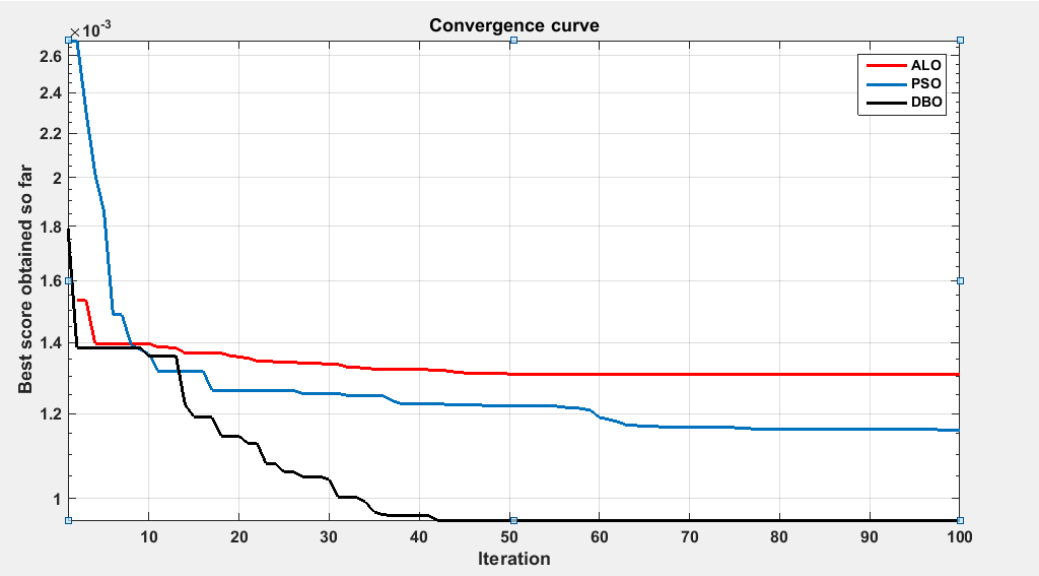


Figure 8. Fitness convergence.

The DBO algorithm is a distinctive optimization approach that consists of six main phases, outlined as follows [40]:

1. **Initialization:** This phase involves setting up the beetle swarm and defining the algorithm parameters.
2. **Fitness Evaluation:** The fitness values are calculated using the objective function.
3. **Update Dung Beetles' Locations:** The positions of all dung beetles are updated according to the algorithm.
4. **Boundary Check:** The boundary of each agent is checked to ensure it remains within the defined boundaries.
5. **Update Optimal Solution:** The current optimal solution and its final fitness value are recorded.
6. **Repeat:** The preceding stages are repeated until the end condition is met.

4.2. Implementation of DBO with Proposed Model

While implementing DBO technique to tune the FOPID controller, which is used as a secondary controller for the proposed complex power network, the following steps were used to tune the controller gain parameters.

4.2.1. Step1: Configure the FOPID Controller

The proposed FOPID controller has three gain parameters (K_P, K_I, K_D) and two fractional values are associated with integral and derivative gain parameters (λ and μ). These five variables must be optimized.

4.2.2. Step 2: Initialization of Objective Function

Establishing an objective function that the DBO will minimize is the fundamental step in the optimization process. The system's performance is measured by this function. The Integral Time Absolute Error (ITAE) is a frequently used objective function and is defined as follows:

$$\text{ITAE} = \int_0^T t\,|e(t)|\,dt \tag{13}$$

where T is the simulation time and e(t) is the Area Control Error (ACE). Finding the set of FOPID settings that minimizes the ITAE is the aim of the DBO.

4.2.3. Step 3: Implement the Dung Beetle Optimizer (DBO)

The DBO algorithm is a meta-heuristic optimization method that draws inspiration from dung beetle behavior. The DBO algorithm must be implemented in a MATLAB 2024a script. The following tasks will be carried out by the script:

Initialization: Start a dung beetle population at random. A collection of FOPID parameters is represented by the position vector of each dung beetle: [K_P, K_I, K_D, λ, μ].

Fitness Evaluation: Run the Simulink model and determine the ITAE for every dung beetle (i.e., for every set of parameters). The "fitness" of the dung beetle's location is indicated by its ITAE value.

Update Positions: The DBO's unique rules, which simulate various dung beetle actions including rolling a dung ball, looking for food, or reproducing, are used by the algorithm to update each dung beetle's position.

Iteration: Until a stopping criterion is satisfied, or for a predetermined number of iterations, the fitness evaluation and position updating procedure is repeated.

Locate the Best Answer: The algorithm finds the dung beetle with the lowest ITAE value at the end of the iterations. The ideal FOPID parameters for the LFC problem are represented by the location of this dung beetle.

4.2.4. Step 4: Incorporate DBO with Simulink Model

The primary loop of your DBO script will resemble the following:

1. Initialize DBO's parameters
   Population = 50
   Iteration = 100.
   Decision vector: x = [K_p, K_i, K_d, λ, μ]X
   Typical bounds: $K_p \in [0, 10]$, $K_i \in [0, 10]$, $K_d \in [0, 10]$. λ and $\mu \in [0, 1]$
2. Primary optimization loop started.
3. For every population of dung beetles:
   In the MATLAB workspace, assign the dung beetle's location to the FOPID controller variables (K_p = position(1), for example).
   Determine the ITAE using the results of the simulation.
4. Using the DBO algorithm, update each dung beetle's location.
5. Continue until the termination requirement is satisfied.

4.3. Cause of Selecting the DBO for FOPID Controller

1. DBO is better for tuning the FOPID controller because it has a robust global search process, fast convergence, and robustness in terms of handling the nonlinear systems.
2. FOPID controller has fractional orders like λ and μ. DBO can able to handle the high-dimensional search effectively.
3. In general, the DBO-tuned FOPID controller provides better results, such as fast settling and smaller steady state error. DBO minimize the ITAE objective effectively.
4. DBO is better over GA, PSO, ACO, DE, and GWO in terms of faster convergence, higher accuracy, better stability, and reduced computational burden.
5. It is robust for step load changes and renewable intermittency.

The DBO algorithm is employed to fine-tune the controller gain parameters for the proposed controller in the investigated power network. The optimized controller gain parameters are presented in Table 1.

Table 1. DBO optimized FOPID controller's parameters.

Optimized Parameters/Optimizer	K_p	K_i	K_d	λ	μ
FOPID controller 1	9.7532	10	9.848	0.7518	1
FOPID controller 2	10	9.96831	8.6514	0.964	0.735

5. Results and Discussion

The frequency stability characteristics of the DBO-FOPID controller within the proposed power network were examined using MATLAB simulation. The controller's performance was assessed by applying a predetermined load profile in area 1. The DBO optimizer was employed to tune the controller's gain parameters, as shown in Table 1. The controller takes the error signal from the system frequency as its input, and based on this signal, generates a refined control signal. This control signal allows each power unit in the network to adjust its power output in order to meet the load demand. The variations in power output for each power unit are shown in Figure 9, while the system's load profile is presented in Figure 10.

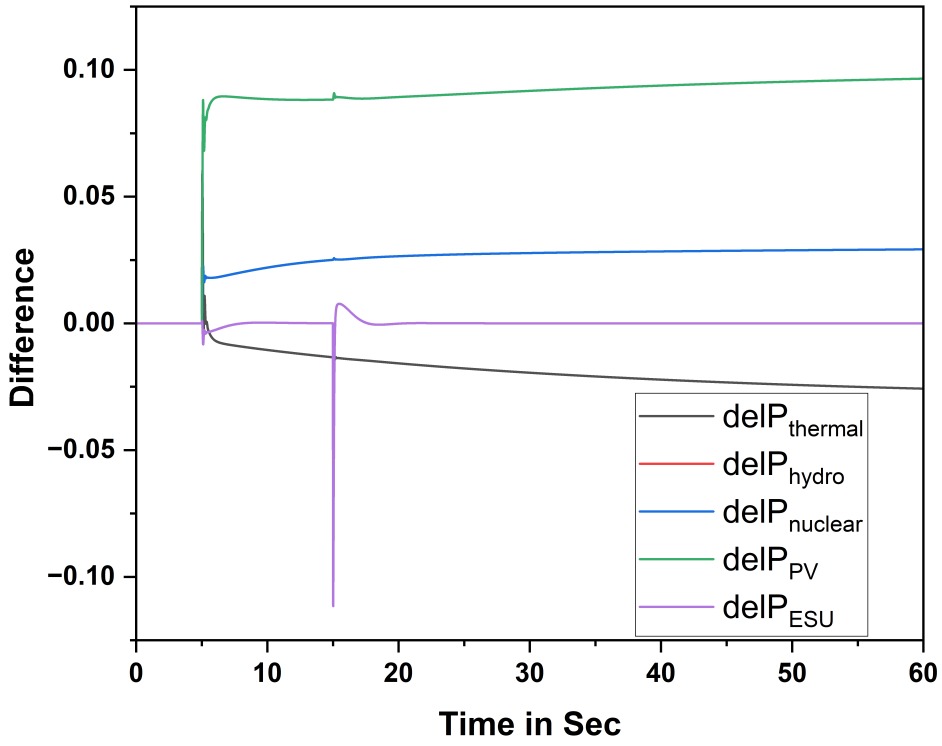


Figure 9. Power changes from each source.

To regulate the frequency fluctuations in areas 1 and 2, as well as the tieline power flow during load change in area 1, system behavior has been analyzed. The detailed analysis is segregated into two cases. Cases 1,2, and 3 concern controller behavior analyses with different optimization techniques, namely, PSO, ALO, and DBO, respectively. Case 4 concerns a performance analysis of the optimization algorithms with superior secondary controllers such as the PSO, ALO, and DBO techniques.

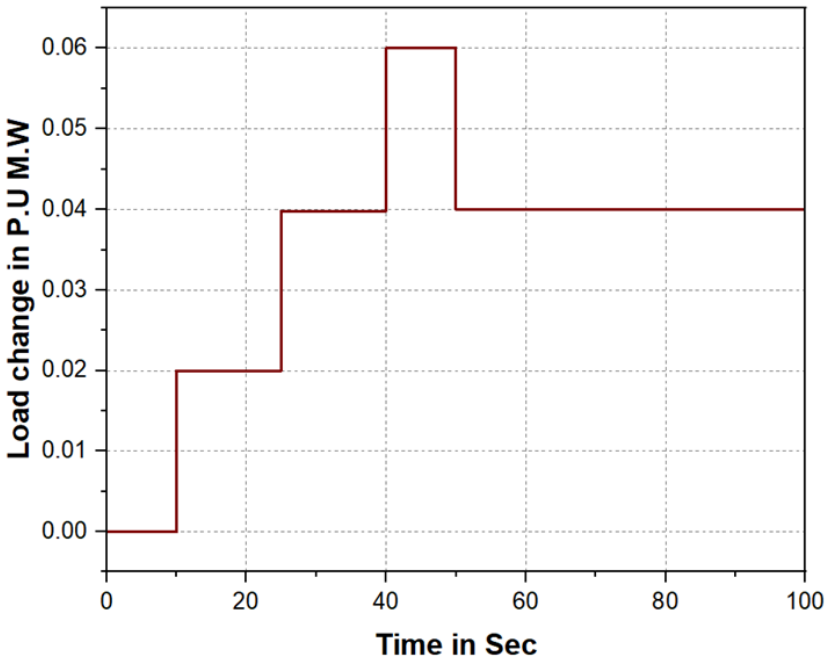


Figure 10. Load profile.

5.1. Case 1: PD, PID, and FOPID Controller Performance Analysis with PSO

In this case, different controllers were utilized to regulate the frequency oscillations. Those controllers are optimized with the PSO technique. The dynamic response comparison of areas 1 and 2 and the tieline power is compared graphically and shown in Figures 11–13. Numerical values of the result are reported in Table 2. The controlled time domain parameters include settling time (Ts), maximum overshoot (P_oS), and minimum undershoot (P_uS).

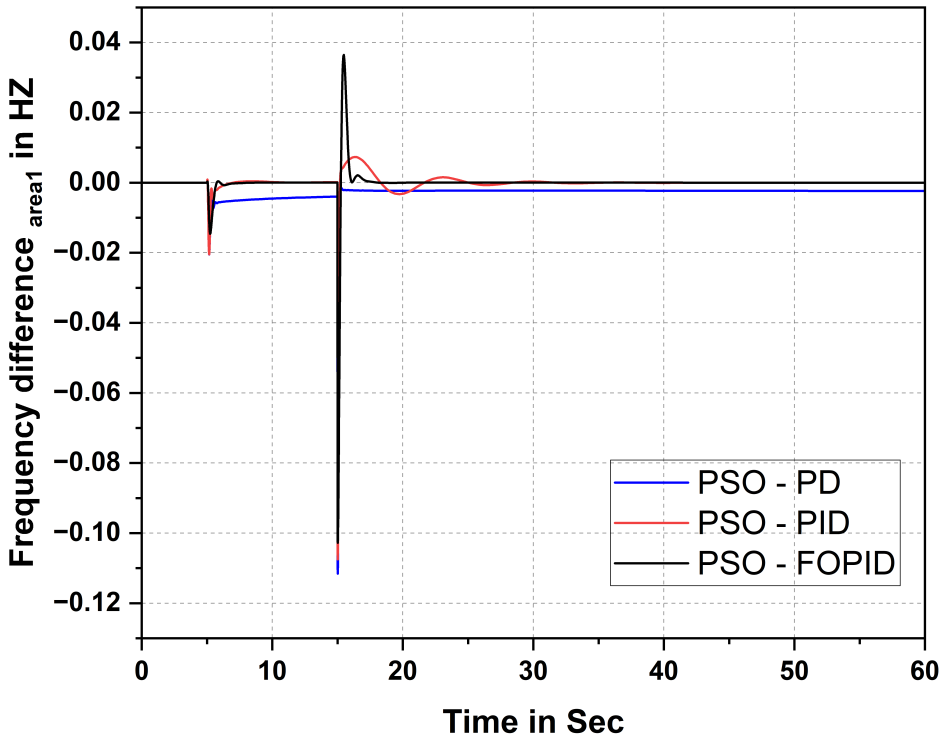


Figure 11. Area 1 frequency oscillation of PSO—PD, PID, and FOPID controller.

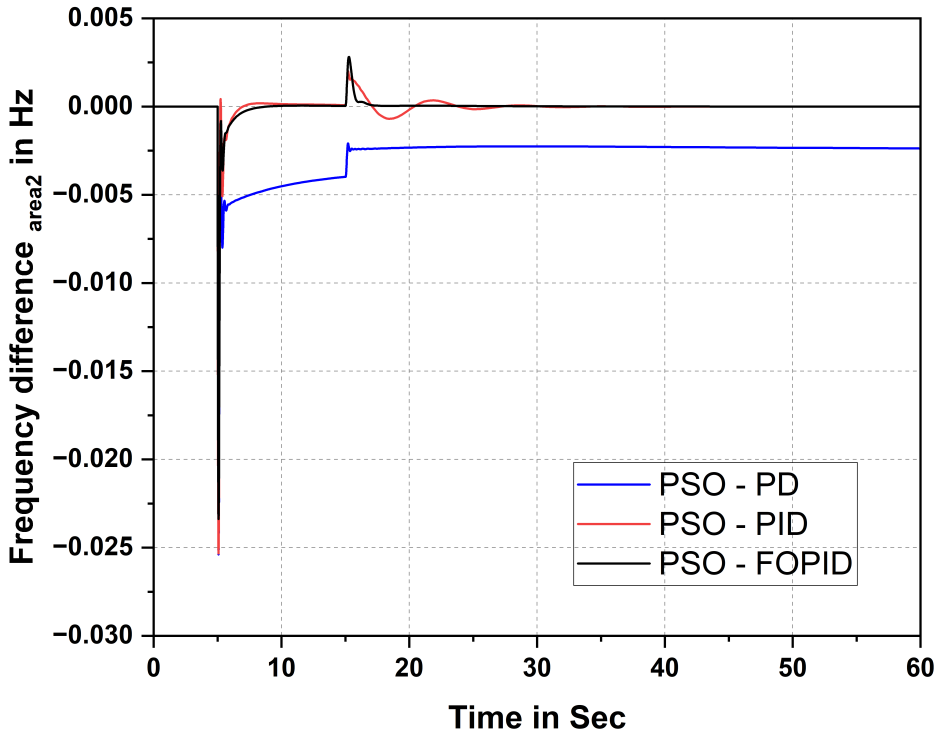


Figure 12. Area 2 frequency oscillation of PSO—PD, PID, and FOPID controller.

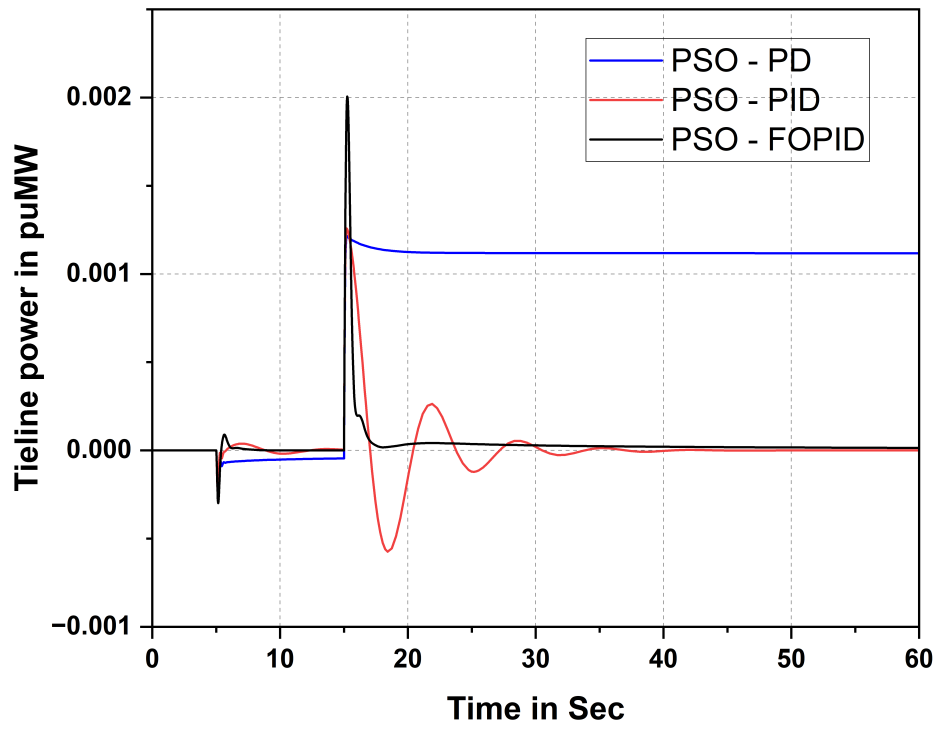


Figure 13. Tieline power oscillation of PSO—PD, PID, and FOPID controllers.

The dynamic control response of the controllers was compared. The PD controller is unsuitable for system frequency regulation. It cannot control the frequency deviation during the period of the load disturbance. However, the remaining two controllers, PID and FOPID, responded well against the frequency oscillation. The PID controller settled the deviation at 37 s in area 1 frequency, 28 s in area 2 frequency, and 45 s in tieline power. The FOPID controller provides a better response than the other two controllers. It settled

the system frequency deviation in area 1 is 21 s, area 2 is 23 s, and tieline power is in 60 s. This is somewhat greater than the PID controller. Thus, the FOPID controller performs partially well, but needs to be optimized further. The improvement of the PSO-tuned FOPID controller over PD and PID controllers, expressed as percentages, is given in Table 3.

Table 2. Optimized parameters using PSO—PD, PID, and FOPID controllers.

Controller	ΔF_1			ΔF_2			ΔP_{tie}		
	T_s (s)	P_oS (10^{-2} Hz)	P_uS (10^{-1} Hz)	T_s (s)	P_oS (10^{-3} Hz)	P_uS (10^{-2} Hz)	T_s (s)	P_oS (10^{-3} puMW)	P_uS (10^{-4} puMW)
PD	∞	0.089	1.1	∞	0.0	2.5	∞	1.2	2.4
PID	37	0.073	1.0	28	2.0	2.5	60	1.2	5.7
FOPID	21	3.6	1.0	23	2.8	2.3	45	2.0	2.9

Table 3. Percentage improvement in settling time (T_s) achieved by PSO-tuned FOPID controller compared with PD and PID.

Optimizer	ΔF_1 (%)	ΔF_2 (%)	ΔP_{tie} (%)
FOPID over PD	-	-	-
FOPID over PID	43	18	33

Figures 11–13 show the controlled response of the frequency of areas 1 and 2 and tieline power, respectively. Tables 2 and 3 demonstrate the superior power of the FOPID controller against frequency oscillation. The FOPID controller performed 43% in area 1, 18% in area 1 frequency, and 33% in tieline power flow. The PSO–FOPID controller is better than the PD and PID controllers.

5.2. Case 2: PD, PID, and FOPID Controller Performance Analysis with ALO

The ALO-tuned PD, PID, and FOPID controllers' performance against frequency oscillations is analyzed. The graphical comparison of areas 1 and 2 and tieline power is plotted and reported in Figures 14–16. Table 4 shows the nominal values of the controller's result.

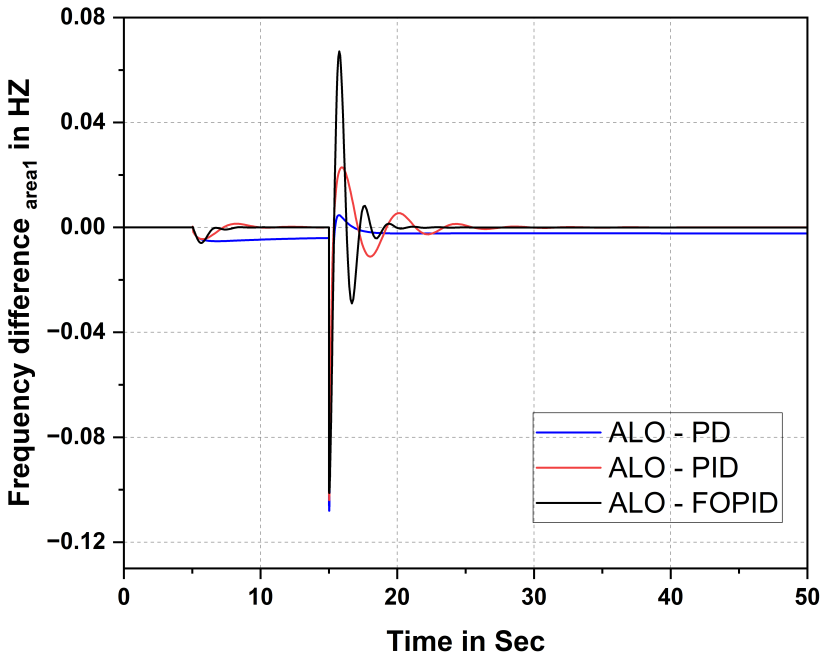


Figure 14. Area 1 frequency oscillation of ALO—PD, PID, and FOPID controller.

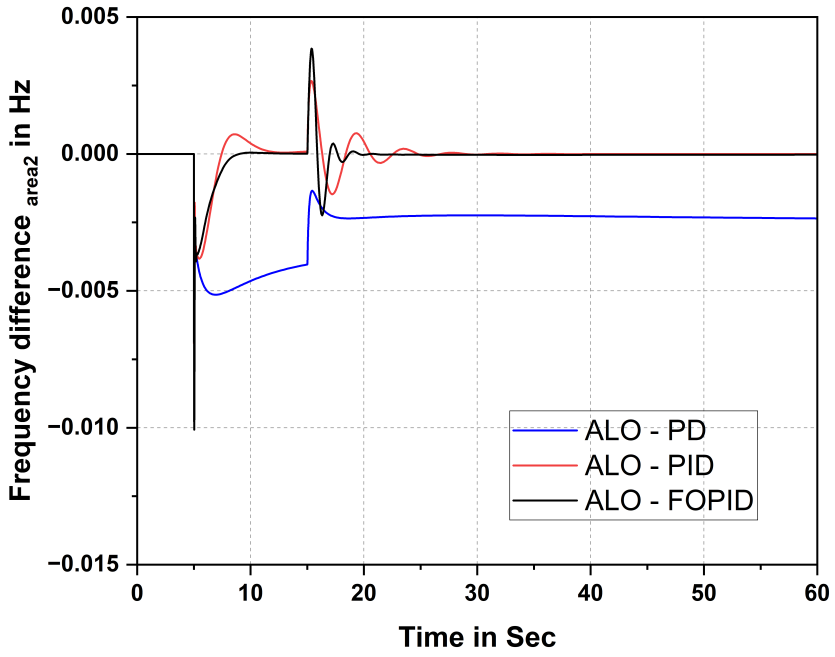


Figure 15. Area 2 frequency oscillation of ALO—PD, PID, and FOPID controller.

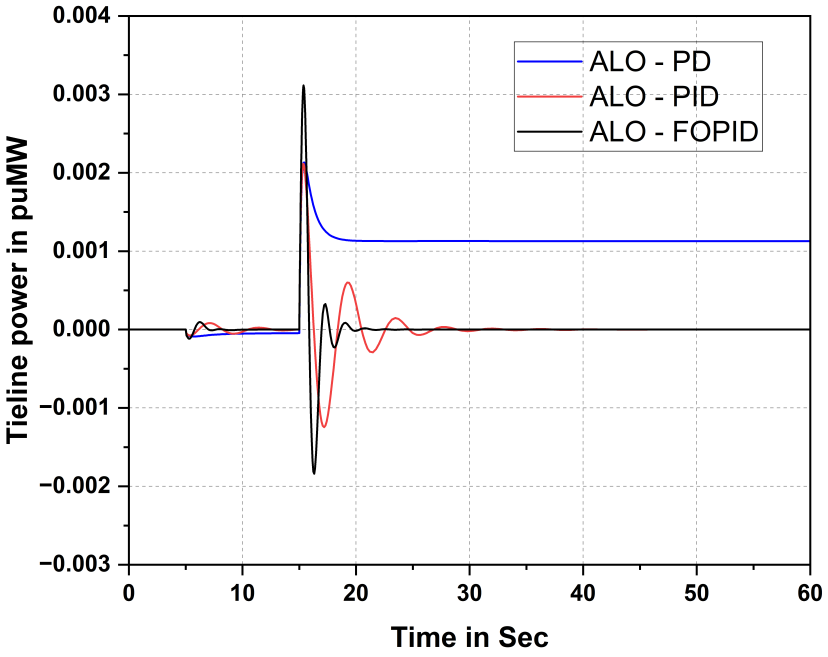


Figure 16. Tieline power oscillation of ALO—PD, PID and FOPID controller.

Compared to the PD and PID controllers' performance against frequency oscillation, the FOPID controller provides a better response. As in the previous case, the PD controller cannot control and maintain the system's frequency stability. However, the PID controller brings the system frequency and tieline power to the nominal in 30 s in area 1, 28 s in area 1, and 40 s in the tieline. The FOPID controller controls the deviations of the frequency of areas 1 and 2 in 20 s, the tieline also in 20 s. Overall, the FOPID controller is better than the PD and PID controllers. The improvement of the ALO-tuned FOPID controller over PD and PID controllers in terms of percentage is given in Table 5.

Table 4. Optimized parameters using ALO—PD, PID, and FOPID controllers.

Controller	ΔF_1			ΔF_2			ΔP_{tie}		
	T_s (s)	P_oS (10^{-3} Hz)	P_uS (10^{-1} Hz)	T_s (s)	P_oS (10^{-3} Hz)	P_uS (10^{-3} Hz)	T_s (s)	P_oS (10^{-3} puMW)	P_uS (10^{-3} puMW)
PD	∞	0.46	1.0	∞	0.0	8.8	∞	2.1	0.089
PID	30	2.2	1.0	28	2.6	8.8	40	2.1	1.2
FOPID	20	6.6	1.0	20	3.8	10.0	20	3.1	1.8

Table 5. Percentage improvement in settling time (T_s) achieved by ALO-tuned FOPID controller compared with PD and PID.

Optimizer	ΔF_1 (%)	ΔF_2 (%)	ΔP_{tie} (%)
FOPID over PD	-	-	-
FOPID over PID	33	29	50

The dynamic response of PD, PID, and FOPID controllers are compared in Figures 14–16 and Tables 4 and 5. The graphical and numerical comparisons demonstrate that the ALO-FOPID controller is better than other controllers for frequency regulation. In terms of the percentage of improvement, the ALO-FOPID controller provided 33% at areas 1 and 29% at area 2 frequency deviation and a 50% improvement in tieline power flow. Section 5.3 discusses the performance of the DBO-tuned controllers.

5.3. Case 3: PD, PID, and FOPID Controller Performance Analysis with DBO

DBO-tuned PD, PID, and FOPID controllers' performance for automatic generation control was compared in this case. The dynamic response of the controllers was compared in both graphical and numerical terms. Figures 17–19 are the graphical comparison of areas 1 and 2 frequency and tieline power flow. Table 6 shows the nominal values of the comparison graphs.

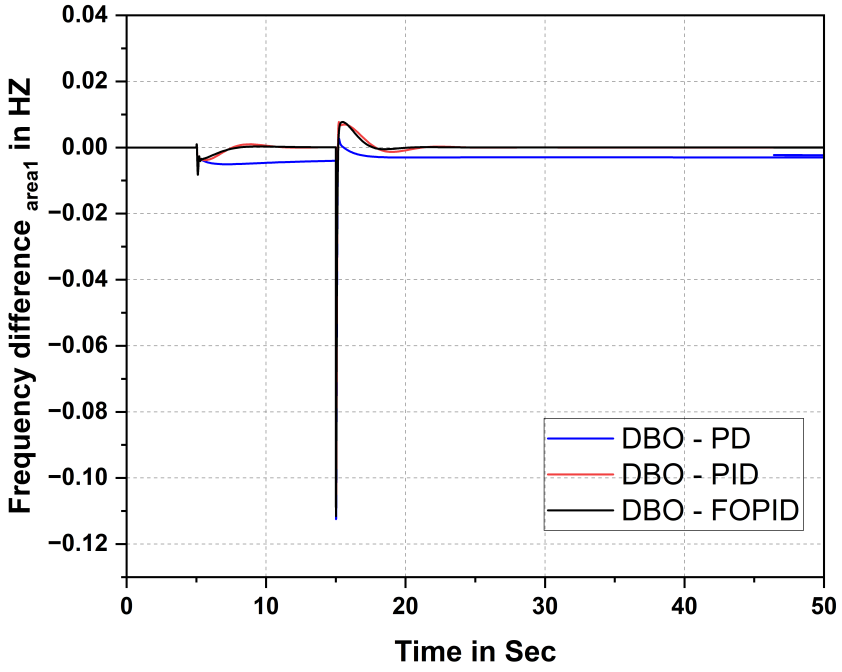


Figure 17. Area 1 frequency oscillation of DBO—PD, PID, and FOPID controller.

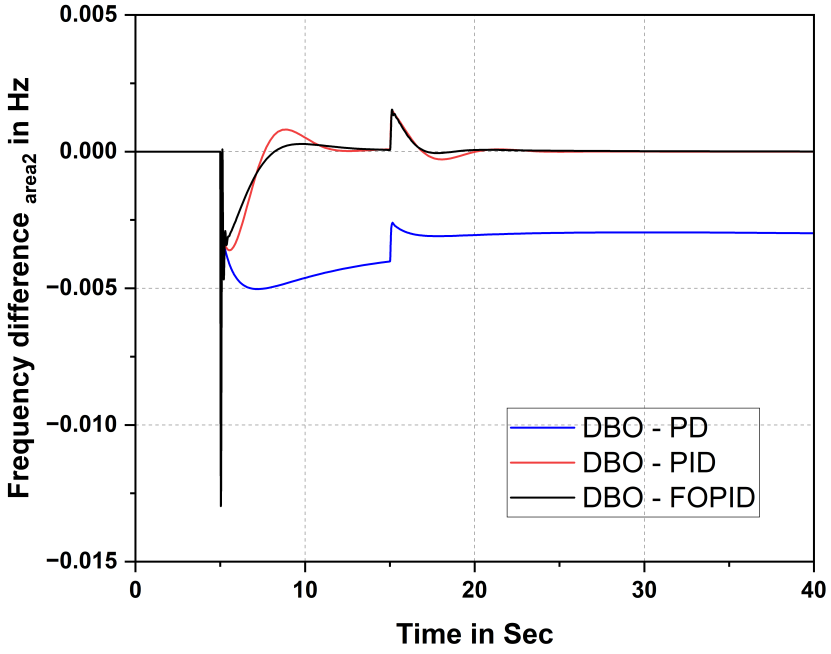


Figure 18. Area 2 frequency oscillation of DBO—PD, PID, and FOPID controller.

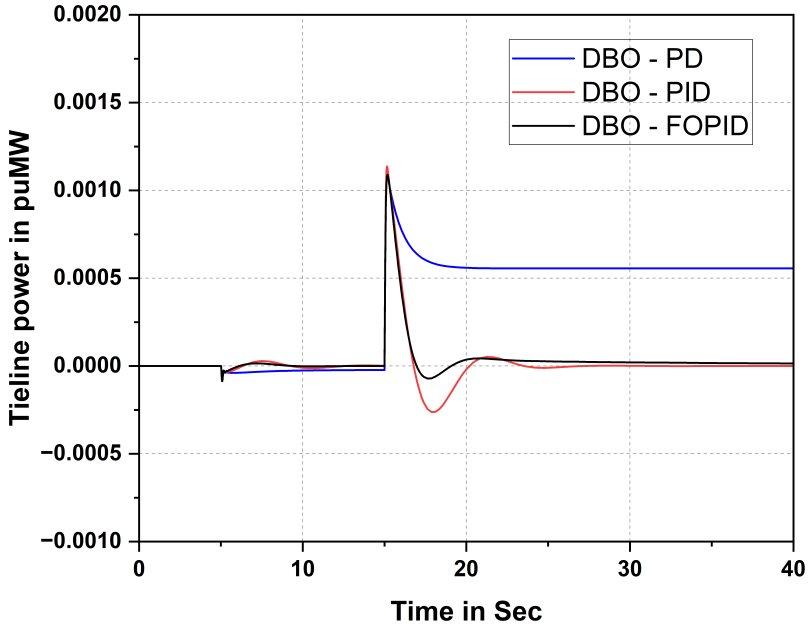


Figure 19. Tie line power oscillation of DBO—PD, PID, and FOPID controller.

The performance of the DBO-tuned PD, PID, and FOPID controllers is analyzed. As in the previous cases, the PD controller is not able to control the frequency deviation. The PID controller stabilizes the frequency of area 1 in 21 s, area 2 in 23 s, and the tieline power in 27 s. Similarly, the FOPID controller stabilizes area 1 in 19 s, area 2 in 19 s, and tieline power in 20 s. The FOPID controller is better than the other two controllers. The improvement of the FOPID controller over PD and PID controllers in terms of percentage is given in Table 7.

Table 6. Optimized parameters using DBO—PD, PID, and FOPID controllers.

Controller	ΔF_1			ΔF_2			ΔP_{tie}		
	T_s (s)	P_oS (10^{-3} Hz)	P_uS (10^{-1} Hz)	T_s (s)	P_oS (10^{-3} Hz)	P_uS (10^{-3} Hz)	T_s (s)	P_oS (10^{-3} puMW)	P_uS (10^{-5} puMW)
PD	∞	2.7	1.2	∞	0.0	8.3	∞	1.1	4.3
PID	21	7.3	1.0	23	1.4	8.3	27	1.3	26.0
FOPID	19	7.7	1.1	19	1.5	12.0	20	1.0	8.6

Table 7. Percentage improvement in settling time (T_s) achieved by FOPID controller compared with PD and PID.

Optimizer	ΔF_1 (%)	ΔF_2 (%)	ΔP_{tie} (%)
FOPID over PD	-	-	-
FOPID over PID	9.5	17.3	26

Figures 17–19, similarly Tables 6 and 7, explain in detail the supremacy of the performance of the DBO—FOPID controller over and PID controllers against frequency difference during the period of the unexpected loading. The DBO—FOPID controller improved the performance 9.5% in area 1 and 17.3% in area 2, and 26% in tieline power. This is a notable performance improvement against oscillations. Sections 5.1–5.3 demonstrate that the PSO-, ALO-, and DBO-tuned FOPID controllers performed better than other controllers.

5.4. Performance Comparison of the PSO-, ALO-, and DBO-Tuned FOPID Controllers

As a final analysis, the best controllers from each case were compared to identify the superior controller for the proposed power system. As per the discussion in the previous cases, the FOPID controller has performed well over PD and PID controllers, so in this case, all three FOPID controllers' results are compared to find the suitable optimizer to maintain the system stability during the period of load oscillation. Figures 20–22 show the graphical comparison. Table 8 shows the numerical values from Figures 20–22.

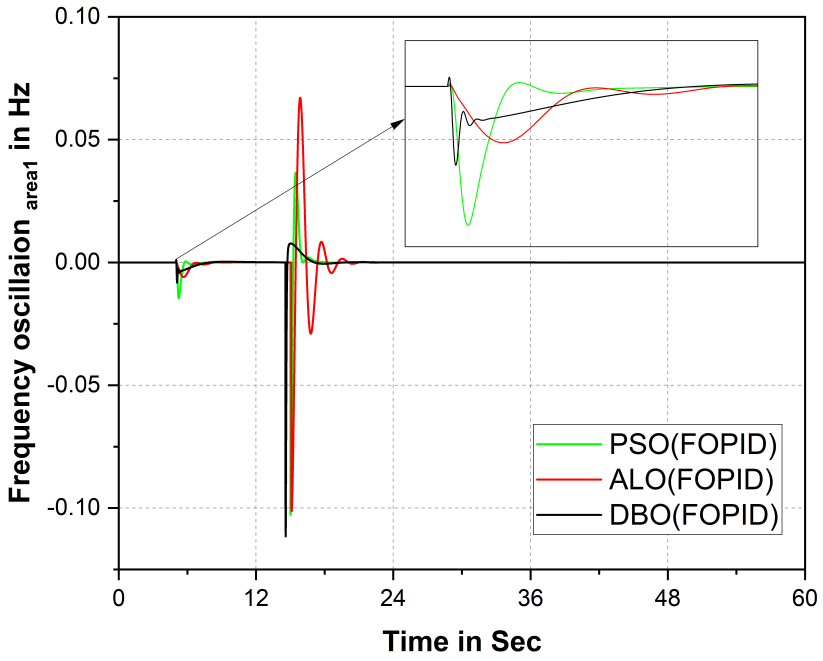


Figure 20. Del F_1 response comparison of PSO, ALO, and DBO—FOPID.

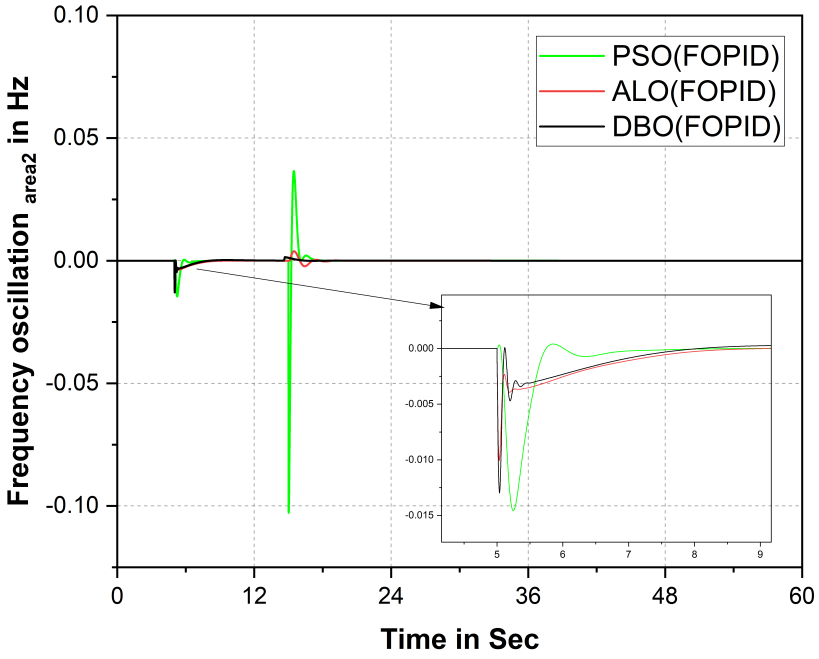


Figure 21. Del F_2 response comparison of PSO, ALO, and DBO—FOPID.

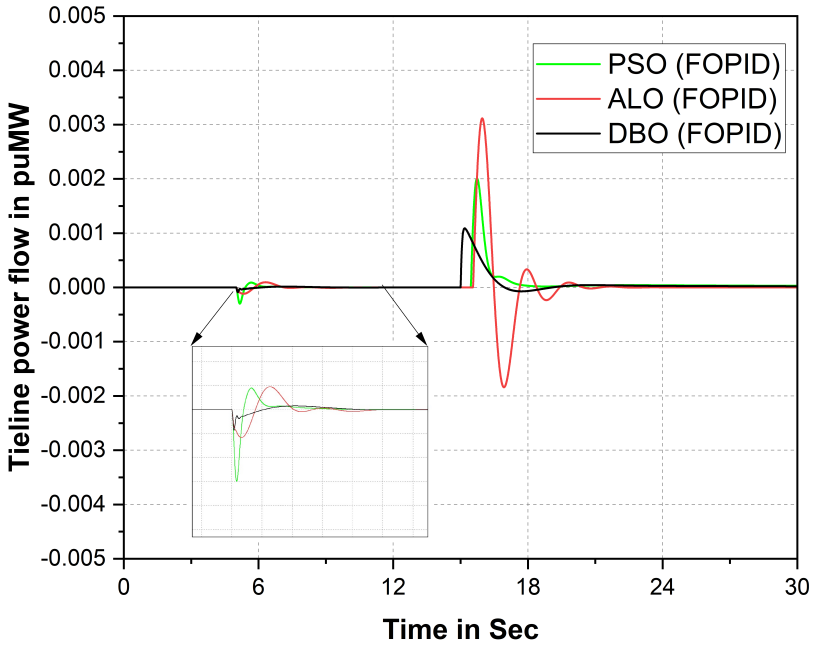


Figure 22. Del $P_{tieline}$ response comparison of PSO, ALO, and DBO—FOPID.

A side-by-side comparison of del F_1, del F_2, and del $P_{tieline}$ demonstrated that the DBO-FOPID controller surpassed both the PSO- and ALO-tuned FOPID controllers in effectiveness. The system frequency drifted away from its nominal value because of fluctuations in load. Throughout the first load fluctuation, the system frequency and tieline power displayed comparatively minor deviations when set against later fluctuations. The highest spike in the system frequency took place during the greatest load fluctuation.

In area 1, the DBO-FOPID controller demonstrated faster restoration of frequency oscillation (del F1) to the standard values compared to the PSO and ALO methods (19 s < 20 s < 21 s). Similar trends were observed for frequency deviation (del F2) (19 s < 20 s < 19 s) and tieline power deviation (delPtieline) (20 s = 20 s < 60 s). Both graph-

ical and numerical comparisons confirmed that the DBO-FOPID controller exhibited superior system frequency stability compared to the PSO and ALO methods.

Table 9 provides detailed information on the percentage improvement of the DBO optimizer in terms of settling time (Ts) compared to the other optimizers.

Table 8. Performance comparison of PSO-, ALO-, and DBO-tuned FOPID controllers.

Algorithm	ΔF_1			ΔF_2			ΔP_{tie}		
	T_s (s)	P_oS (10^{-2} Hz)	P_uS (10^{-1} Hz)	T_s (s)	P_oS (10^{-3} Hz)	P_uS (10^{-2} Hz)	T_s (s)	P_oS (10^{-3} puMW)	P_uS (10^{-4} puMW)
PSO	21	3.6	1.0	23	2.8	2.3	60	2.0	2.9
ALO	20	6.6	1.0	20	3.8	1.0	20	3.1	18.0
DBO	19	0.77	1.1	19	1.5	1.2	20	1.0	0.86

Table 9. Percentage improvement in settling time (T_s) achieved by DBO compared with PSO and ALO.

Optimizer	ΔF_1 (%)	ΔF_2 (%)	ΔP_{tie} (%)
DBO over PSO	9.5	17.3	66.6
DBO over ALO	4.7	4.7	66.6

In Section 5.1, PSO-tuned FOPID controller performance was compared with that of PD and PID controllers. The comparison in terms of both graphical and numerical comparisons showed that the PSO—FOPID controller performs well. Similarly, Sections 5.2 and 5.3 analyze the ALO- and DBO—tuned FOPID controllers. In all cases, the FOPID controller performs better than the PD and PID controllers. Finally, all three techniques (PSO, ALO, and DBO)-tuned FOPID controllers were compared in Section 5.4. In conclusion, the overall comparison indicates that the DBO-FOPID controller offers enhanced control performance in mitigating frequency oscillation under unexpected loading conditions.

6. Conclusions

In this research, the effectiveness of the FOPID controller within the secondary loop of the proposed power network was assessed. Controller parameters were tuned using the Dung Beetle Optimizer (DBO) to strengthen control action against frequency fluctuations. The findings indicated that the proposed DBO-FOPID controller surpassed the PSO- and ALO-tuned FOPID controllers in terms of performance. Under abrupt loading conditions, the frequency of the interconnected power network and power flow across the tieline were successfully stabilized. The efficacy of the DBO-FOPID controller was validated through multiple comparisons, encompassing both graphical and numerical forms. The comprehensive conclusion of the work can be outlined as follows:

- The performance of the PSO—tuned FOPID controller is studied in case 1. The FOPID controller provided improvements of 43%, 18%, and %33, respectively, in areas 1 and 2 and tieline.
- The superiority of the ALO—tuned FOPID controller is investigated in case 2. This shows that the FOPID controller more quickly regulated the oscillation than the PID controller. The percentage improvement was 33%, 29%, and 50% in areas 1 and 2 and tieline power, respectively.
- In case 3, the performance of the DBO—FOPID controller over PD and PID controllers is investigated. The FOPID controller settled the oscillation and provided 9.5%, 17.3%, and 26% improvement over the PID controller.
- Finally, the performance of PSO- and ALO-tuned FOPID controllers was compared with that of the DBO—tuned FOPID controller. The DBO—tuned FOPID controller

improved the regulation over the PSO-tuned FOPID controller by 9.5%, 17.3%, and 26%, and over the ALO-tuned FOPID controller by 4.7%, 4.7%, and 66.6%.

Author Contributions: Conceptualization, B.D. and J.K.; methodology, B.D. and J.K.; software, S.S.; validation, A.B. and B.D.; formal analysis, B.D.; investigation, A.B.; writing—original draft preparation, B.D. and J.K.; writing—review and editing, B.D., J.K., and S.K.M.; supervision, A.B. All authors have read and agreed to the published version of the manuscript.

Funding: This research received no external funding.

Institutional Review Board Statement: Not applicable.

Informed Consent Statement: Not applicable.

Data Availability Statement: The data presented in this study are available on request from the corresponding author due to privacy.

Conflicts of Interest: The authors declare no conflict of interest.

References

1. Veerasamy, V.; Wahab, N.I.A.; Ramachandran, R.; Othman, M.L.; Hizam, H.; Kumar, J.S.; Irudayaraj, A.X.R. Design of single- and multi-loop self-adaptive PID controller using heuristic based recurrent neural network for ALFC of hybrid power system. *Expert Syst. Appl.* **2022**, *192*, 116402. [CrossRef]
2. Qu, Z.; Younis, W.; Liu, X.; Junejo, A.K.; Almutairi, S.Z.; Wang, P. Optimized PID Controller for Load Frequency Control in Multi-Source and Dual-Area Power Systems Using PSO and GA Algorithms. *IEEE Access* **2024**, *12*, 186658–186678. [CrossRef]
3. Boopathi, D.; Jagatheesan, K.; Anand, B.; Kumarakrishnan, V.; Samanta, S. Effect of sustainable energy sources for load frequency control (LFC) of single-area wind power systems. In *Industrial Transformation*; CRC Press: Boca Raton, FL, USA, 2022; pp. 87–98.
4. Yameen, M.Z.; Junejo, A.K.; Lu, Z.; Siddiqui, R.A.; El-Sousy, F.F.; Naveed, I. Hybrid GOA and PSO optimization for load frequency control in renewable multi-source dual-area power systems. *Sci. Rep.* **2025**, *15*, 17549. [CrossRef]
5. Barakat, M.; Donkol, A.; Hamed, H.F.; Salama, G.M. Harris hawks-based optimization algorithm for automatic LFC of the interconnected power system using PD–PI cascade control. *J. Electr. Eng. Technol.* **2021**, *16*, 1845–1865. [CrossRef]
6. Ogar, V.N.; Hussain, S.; Gamage, K.A. Load frequency control using the particle swarm optimisation algorithm and PID controller for effective monitoring of transmission line. *Energies* **2023**, *16*, 5748. [CrossRef]
7. Choudhary, R.; Rai, J.N.; Arya, Y. Cascade FOPI-FOPTID controller with energy storage devices for AGC performance advancement of electric power systems. *Sustain. Energy Technol. Assess.* **2022**, *53*, 102671. [CrossRef]
8. Ebrahim, M.A.; Becherif, M.; Abdelaziz, A.Y. PID/FOPID-based frequency control of zero-carbon multi sources-based interconnected power systems under deregulated scenarios. *Int. Trans. Electr. Energy Syst.* **2021**, *31*, e12712. [CrossRef]
9. Babaei, F.; Lashkari, Z.B.; Safari, A.; Farrokhifar, M.; Salehi, J. Salp swarm algorithm-based fractional-order PID controller for LFC systems in the presence of delayed EV aggregators. *IET Electr. Syst. Transp.* **2020**, *10*, 259–267. [CrossRef]
10. Sondhi, S.; Hote, Y.V. Fractional order PID controller for load frequency control. *Energy Convers. Manag.* **2014**, *85*, 343–353. [CrossRef]
11. Michael, C.; Tola, O.J.; Nwohu, M.N.; Ambafi, J.G. Load Frequency Control of a Microgrid using Fractional Order PID Controller. In *Proceedings of the 2022 IEEE Nigeria 4th International Conference on Disruptive Technologies for Sustainable Development (NIGERCON), Abuja, Nigeria, 15–17 May 2022*; IEEE: New York, NY, USA, 2022; pp. 1–6. [CrossRef]
12. Fathy, A.; Yousri, D.; Rezk, H.; Thanikanti, S.B.; Hasanien, H.M. A Robust Fractional-Order PID Controller Based Load Frequency Control Using Modified Hunger Games Search Optimizer. *Energies* **2022**, *15*, 361. [CrossRef]
13. Elsaied, M.M.; Abdel Hameed, W.H.; Hasanien, H.M. Frequency stabilization of a hybrid three-area power system equipped with energy storage units and renewable energy sources. *IET Renew. Power Gener.* **2022**, *16*, 3267–3286. [CrossRef]
14. Irudayaraj, A.X.R.; Wahab, N.I.A.; Umamaheswari, M.G.; Radzi, M.A.M.; Sulaiman, N.B.; Veerasamy, V.; Prasanna, S.C.; Ramachandran, R. A Matignon's Theorem Based Stability Analysis of Hybrid Power System for Automatic Load Frequency Control Using Atom Search Optimized FOPID Controller. *IEEE Access* **2020**, *8*, 168751–168772. [CrossRef]
15. Mohammadikia, R.; Aliasghary, M. A fractional order fuzzy PID for load frequency control of four-area interconnected power system using biogeography-based optimization. *Int. Trans. Electr. Energy Syst.* **2019**, *29*, e2735. [CrossRef]
16. Kumar, N.; Alotaibi, M.A.; Singh, A.; Malik, H.; Nassar, M.E. Application of Fractional Order-PID Control Scheme in Automatic Generation Control of a Deregulated Power System in the Presence of SMES Unit. *Mathematics* **2022**, *10*, 521. [CrossRef]

17. Gorripotu, T.S.; Samalla, H.; Jagan Mohana Rao, C.; Azar, A.T.; Pelusi, D. TLBO Algorithm Optimized Fractional-Order PID Controller for AGC of Interconnected Power System. In *Advances in Intelligent Systems and Computing*; Springer: Singapore, 2019; pp. 847–855. [CrossRef]
18. Fayek, H.H. Load Frequency Control of a Power System with 100% Renewables. In *Proceedings of the 54th International Universities Power Engineering Conference (UPEC)*; IEEE: New York, NY, USA, 2019; pp. 1–6. [CrossRef]
19. Morsali, J.; Zare, K.; Tarafdar Hagh, M. Applying fractional order PID to design TCSC-based damping controller in coordination with automatic generation control of interconnected multi-source power system. *Eng. Sci. Technol. Int. J.* **2017**, *20*, 1–17. [CrossRef]
20. Murugesan, D.; Shah, P.; Jagatheesan, K.; Sekhar, R.; Kulkarni, A.J. Cohort intelligence optimization based controller design of isolated and interconnected thermal power system for automatic generation control. In *Proceedings of the 2022 Second International Conference on Computer Science, Engineering and Applications (ICCSEA)*; IEEE: New York, NY, USA, 2022; pp. 1–6. [CrossRef]
21. Kumarakrishnan, V.; Vijayakumar, G.; Boopathi, D.; Jagatheesan, K.; Saravanan, S.; Anand, B. Optimized PSO Technique Based PID Controller for Load Frequency Control of Single Area Power System. Available online: www.solidstatetechnology.us (accessed on 10 July 2026).
22. Ahuja, A.; Narayan, S.; Kumar, J. Robust FOPID controller for load frequency control using Particle Swarm Optimization. In *Proceedings of the 2014 6th IEEE Power India International Conference (PIICON)*; IEEE: New York, NY, USA, 2014; pp. 1–6. [CrossRef]
23. Khezri, R.; Oshnoei, A.; Hagh, M.T.; Muyeen, S.M. Coordination of heat pumps, electric vehicles and AGC for efficient LFC in a smart hybrid power system via SCA-based optimized FOPID controllers. *Energies* **2018**, *11*, 420. [CrossRef]
24. Arya, Y. A novel CFFOPI-FOPID controller for AGC performance enhancement of single and multi-area electric power systems. *ISA Trans.* **2020**, *100*, 126–135. [CrossRef] [PubMed]
25. Naga Sai Kalyan, C.H.; Goud, B.S.; Reddy, C.R.; Udumula, R.R.; Bajaj, M.; Sharma, N.K.; Elgamli, E.; Shouran, M.; Kamel, S. Seagull Optimization Algorithm-Based Fractional-Order Fuzzy Controller for LFC of Multi-Area Diverse Source System with Realistic Constraints. *Front. Energy Res.* **2022**, *10*, 921426. [CrossRef]
26. Elkasem, A.H.A.; Kamel, S.; Korashy, A.; Nasrat, L. Load Frequency Control Design of Two Area Interconnected Power System Using GWO. In *Proceedings of the 2019 IEEE Conference on Power Electronics and Renewable Energy (CPERE)*; IEEE: New York, NY, USA, 2019; pp. 278–283. [CrossRef]
27. Taher, S.A.; Hajiakbari Fini, M.; Falahati Aliabadi, S. Fractional order PID controller design for LFC in electric power systems using imperialist competitive algorithm. *Ain Shams Eng. J.* **2014**, *5*, 121–135. [CrossRef]
28. Barakat, M. Novel chaos game optimization tuned-fractional-order PID fractional-order PI controller for load-frequency control of interconnected power systems. *Prot. Control Mod. Power Syst.* **2022**, *7*, 16. [CrossRef]
29. Ramachandran, R.; Satheesh Kumar, J.; Madasamy, B.; Veerasamy, V. A hybrid MFO-GHNN tuned self-adaptive FOPID controller for ALFC of renewable energy integrated hybrid power system. *IET Renew. Power Gener.* **2021**, *15*, 1582–1595. [CrossRef]
30. Arya, Y. Impact of hydrogen aqua electrolyzer-fuel cell units on automatic generation control of power systems with a new optimal fuzzy TIDF-II controller. *Renew. Energy* **2019**, *139*, 468–482. [CrossRef]
31. Nour, M.; Magdy, G.; Chaves-Avila, J.P.; Sanchez-Miralles, A.; Petlenkov, E. Automatic Generation Control of a Future Multisource Power System Considering High Renewables Penetration and Electric Vehicles: Egyptian Power System in 2035. *IEEE Access* **2022**, *10*, 51662–51681. [CrossRef]
32. Alomoush, M.I. Load frequency control and automatic generation control using fractional-order controllers. *Electr. Eng.* **2010**, *91*, 357–368. [CrossRef]
33. Pan, I.; Das, S. Fractional-order load-frequency control of interconnected power systems using chaotic multi-objective optimization. *Appl. Soft Comput.* **2015**, *29*, 328–344. [CrossRef]
34. Ahmed, M.; Khamies, M.; Magdy, G.; Kamel, S. Designing Optimal PIλDμ Controller for LFC of Two-Area Power Systems Using African Vulture's Optimization Algorithm. In *Proceedings of the 2021 22nd International Middle East Power Systems Conference (MEPCON)*; IEEE: New York, NY, USA, 2021; pp. 430–437. [CrossRef]
35. Mishra, S.; Prusty, U.C.; Prusty, R.C.; Panda, S. Novel load frequency control scheme for hybrid power systems employing interline power flow controller and redox flow battery. *Energy Sources Part A Recover. Util. Environ. Eff.* **2025**, *47*, 11787–11805.
36. Malamaki, K.-N.D.; Fotopoulou, M.; Martinez-Lopez, D.; Lampsidis, G.; Ferrer-Fernandez, P.; Andriopoulos, N.; Tzanis, N.; Kaousias, K.; Chassioti, E.; Moraitis, I. Day ahead optimization of insular systems considering future interconnection: The case of Ikaria island. *Sustain. Energy Grids Netw.* **2025**, *44*, 102018. [CrossRef]
37. Murugesan, D.; Jagatheesan, K.; Boopathi, D. Meta-heuristic Strategy Planned Controller for Frequency Supervision of Integrated Thermal Plant with Renewable Source. In *Proceedings of the 2021 IEEE 3rd PhD Colloquium on Ethically Driven Innovation and Technology for Society (PhD EDITS)*; IEEE: New York, NY, USA, 2021; pp. 1–2. [CrossRef]
38. Dhanasekaran, B.; Siddhan, S.; Kaliannan, J. Ant colony optimization technique tuned controller for frequency regulation of single area nuclear power generating system. *Microprocess. Microsyst.* **2020**, *73*, 102953. [CrossRef]

39. Ahmed, M.; Khamies, M.; Hassan, M.H.; Domínguez-García, J.L.; Kamel, S. A modified controller scheme for frequency stability enhancement of hybrid two-area power grid with renewable energy sources. *IET Renew. Power Gener.* **2023**, *17*, 1035–1067. [CrossRef]
40. Xue, J.; Shen, B. Dung beetle optimizer: A new meta-heuristic algorithm for global optimization. *J. Supercomput.* **2023**, *79*, 7305–7336. [CrossRef]

Disclaimer/Publisher's Note: The statements, opinions and data contained in all publications are solely those of the individual author(s) and contributor(s) and not of MDPI and/or the editor(s). MDPI and/or the editor(s) disclaim responsibility for any injury to people or property resulting from any ideas, methods, instructions or products referred to in the content.